Supplementary information

Zeolitic imidazolate framework (ZIF-8) based polymer nanocomposite membranes for gas separation

Qilei Song,[a] S.K. Nataraj,[a] Mina V. Roussenova,[b] Jin Chong Tan,[c] David J. Hughes,[b] Wei Li,[c] Pierre Bourgoin,[a] Ashraf Alam,[b] Anthony K. Cheetham,[c] Shaheen A. Al-Muhtaseb,[d] Easan Sivaniah [a,*]

[a] *Biological and Soft Systems Sector, Cavendish Laboratory, University of Cambridge, Cambridge CB3 0HE, UK*

[b] *H. H. Wills Physics Laboratory, University of Bristol, Tyndall Avenue, Bristol BS8 1TL, UK*

[c] *Department of Material Science and Metallurgy, University of Cambridge, Cambridge CB2 3QZ, UK*

[d] *Department of Chemical Engineering, Qatar University, P.O. Box 2713, Doha, Qatar*

*Corresponding author

Dr Easan Sivaniah Tel.: +44 1223 337267 Fax.: +44 1223 337000

Email: es10009@cam.ac.uk

This supplementary document contains:

Table S1-S4

Fig. S1-S14.

Table S1. Summary of gas permeation properties of representative Zeolitic imidazolate framework (ZIF) based membranes

Samples	Pore Aperture (Å)	Membrane Thickness (*L*) (μm)	Permeance (*J*) (10^{-8}) mol m^{-2} $s^{-1}Pa^{-1}$					Permeability (*P*) (Barrer)[c]					Selectivity					Ref
			H_2	CO_2	O_2	N_2	CH_4	H_2	CO_2	O_2	N_2	CH_4	CO_2/N_2	CO_2/CH_4	O_2/N_2	H_2/N_2	H_2/CH_4	
Knudsen diffusion													0.8	0.60	0.93	3.7	2.8	[1]
ZIF-7 [a]	3.0	~1.5	7.4	1.1	-	1.1	1.18	331	49	-	49	53	1.0	0.9	-	6.8	6.2	[2]
ZIF-7 [a]	3.0	~2	4.55	0.35	-	0.22	0.31	272	21	-	13	19	1.6	1.1	-	20.9	14.3	[3]
ZIF-8 [a]	3.4	~30	6.04	1.33	1.04	0.52	0.48	5411	1192	932	466	430	2.6	2.8	2.0	11.6	12.6	[4]
ZIF-8 [a]	3.4	~20	17.3	4.45	5.22	1.49	1.33	10333	2658	3118	890	794	3.0	3.3	3.5	11.6	13.0	[5]
ZIF-8 [a]	3.4	~20	8.23	-	1.27	0.69	0.63	4916	-	759	412	376	-	-	1.8	11.9	13.1	[6]
ZIF-22 [a]	3.2	~40	20.2	2.38	2.80	2.84	3.02	24130	2843	3345	3393	3608	0.8	0.8	1.0	7.1	6.7	[7]
ZIF-22 [b]	3.2	~40	(~18.0)	2.30	2.95	2.93	3.31	21502	2747	3524	3500	3954	0.8	0.7	1.0	6.4	5.2	[7]
ZIF-90 [a]	3.5	~20	25.0	3.48	-	1.98	1.57	14932	2079	-	1183	938	1.8	2.2	-	12.6	15.9	[8]
ZIF-90 [b]	3.5	~20	(~24.0)	3.25	-	2.12	1.64	14335	1941	-	1266	980	1.5	2.0	-	11.3	15.3	[8]
ZIF-90 [a]	3.5	~20	21.0	1.34	-	1.28	1.08	12543	800	-	765	645	1.0	1.2	0.0	16.4	19.4	[9]
ZIF-90 [b]	3.5	~20	(~20.0)	1.32	-	1.35	1.03	11946	788	-	806	615	1.0	1.3	0.0	14.8	19.4	[9]

[a] pure gas

[b] mixed gases, data in parenthesis means the average value.

[c] Permeability is calculated from $P=J\times L$. 1 Barrer = 3.348×10^{-16} mol m/ (m^2 s Pa).

Gas permeation apparatus

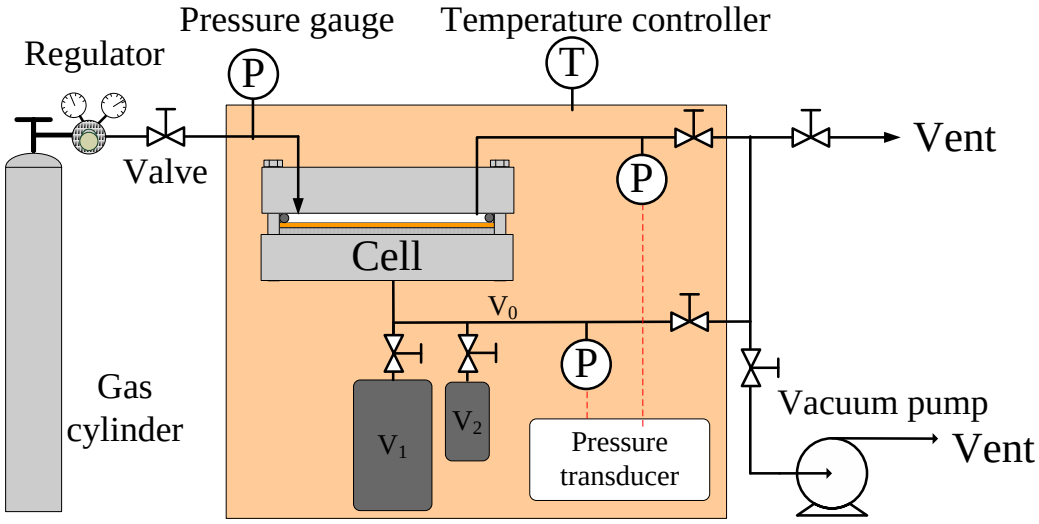

Fig. S1 Schematic diagram of pure gas permeation apparatus. P: pressure gauge or transducer; T: temperature controller; V_0, V_1 and V_2: volume of tube, gas sample cylinder 1 and 2 respectively; The membrane cell could be placed in a temperature controlled box. In this study, the gas permeation was performed at room temperature of 22°C.

A stainless steel membrane holder (Millipore, model XX4404700, diameter of 47 mm) was used as the membrane cell where the membrane was supported on filter paper and a porous metal disk at the bottom. The mass transfer resistance of the support is far less compared to that of the polymer film so that the measured gas flux reflects the inherent gas permeation properties of the membrane. The membrane was sealed by a viton o-ring (instead of silicone o-ring which gave high gas leakage). The effective area of the membrane available for gas diffusion is 12.6 cm^2.

The permeate volume includes the gas sampling cylinder of the tubes, tube connections, valves and the membrane cell. The stainless steel gas sampling cylinder (Swagelok, 75 and 500 cm^3) can be switched to provide reasonable volume depending on the permeability of the membrane. The rate of increase of permeate pressure could be adjusted by the volume. For the low permeability gas, only tube volume is enough to measure the pressure increase rate. The volume (V_0) of tubing and the dead volume in the cell could be calibrated by the mass balance of N_2 at low pressure using standard known volume of V_1 or V_2.

The pure gas was supplied from the gas cylinders with pressure measured by a digital manometer (Keller LEO 2 Ei, absolute pressure 0-31 bar). For the dense membrane, the rate of gas permeation is quite slow, and the permeate pressure is usually set to be lower than 50 mbar with the feeding pressure constant at 4 bar. Therefore, the effective pressure difference between the feeding and permeate could be assumed as constant.

In a typical run, the membrane was loaded in the cell and both upstream and downstream were evacuated for overnight prior to measurement of each gas giving true kinetics data. Then the leak rate was checked by measuring the increase of permeate pressure with the valve connecting the vacuum pump closed. Normally, the leaking rate is negligible with good sealing and evacuation. Then the feed gas was introduced and the feed and permeate pressure were recorded by pressure transmitters (Keller PAA 33X, Accuracy of 0.01% F.S.) connected to a data acquisition system, until the permeate pressure reached steady state (the slope of pressure increase, *dp*/*dt*, became constant). The steady state could be verified by evacuating the downstream briefly and measuring the slope of the permeate pressure again.

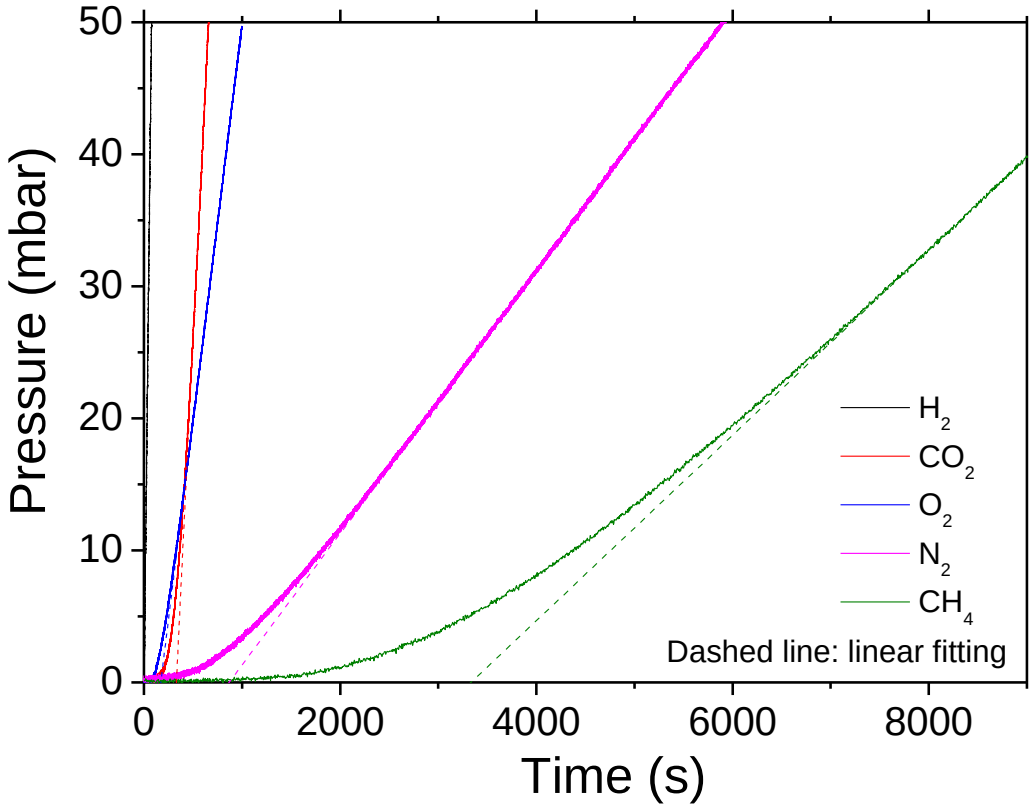

Fig. S2 A representative pressure-time profile of gas permeation for a Matrimid®/ZIF-8-30wt% sample (annealed at 230°C for 18h under vacuum). The dashed lines represent the linear fitting of the steady state. Gas permeation test condition: feeding pressure of 4 bar at room temperature (22°C).

Synthesis of ZIF-8 nanocrystals

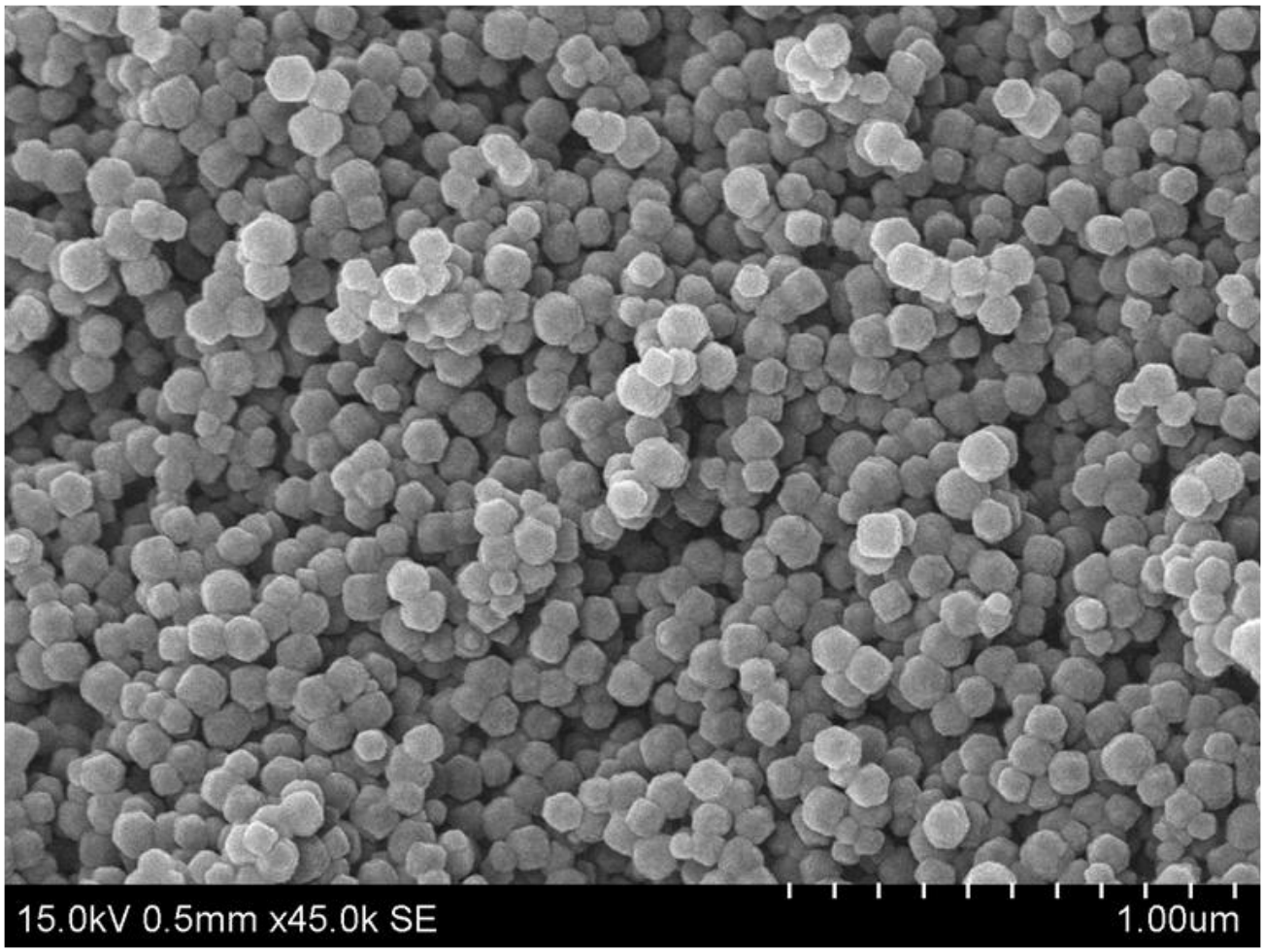

Fig. S3 SEM images of ZIF-8 nanocrystals. The scale bar (1.0μm) is represented by 10 grids.

XRD analyses of ZIF-8 nanocrystals

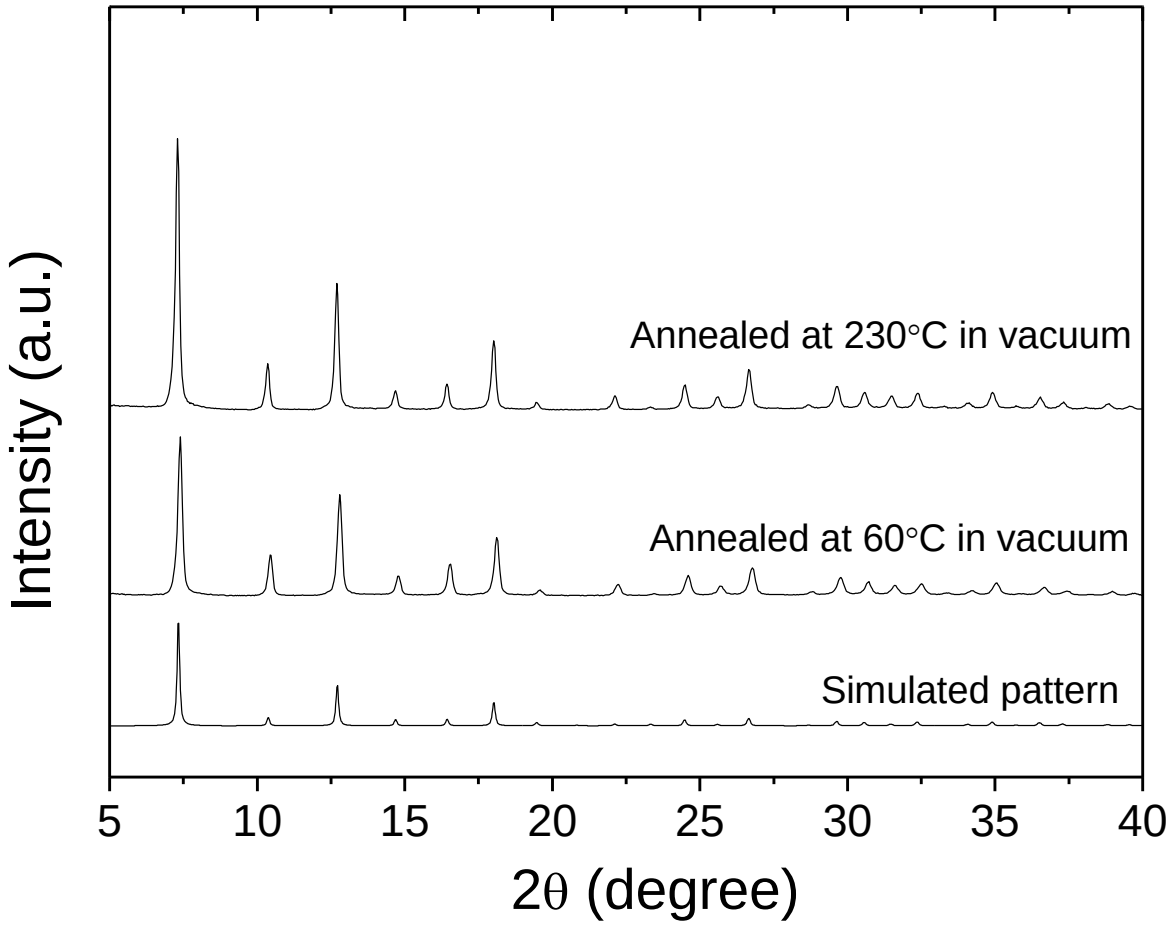

Fig. S4 X-ray diffraction patterns of ZIF-8 nanocrystals. The simulated pattern is also included.[10]

XRD pattern of the ZIF-8 nanocrystals as shown in Fig. S4 matches well with the previous reports and the theoretical pattern.[10-11] The average crystallite size of ZIF-8 nanocrystals is around 70 nm as calculated from the broadening of the peaks using the Scherrer equation, which is in agreement with the direct observation of particle size by SEM and STEM. This size is slightly bigger than that observed in nanocomposite membrane, possibly because of the aggregation of ZIF-8 nanocrystals accompanied with covalent bonding of Zn-imidazole (Him) on the particle surface during annealing process, as proposed by Cravillon *et al.* [11]

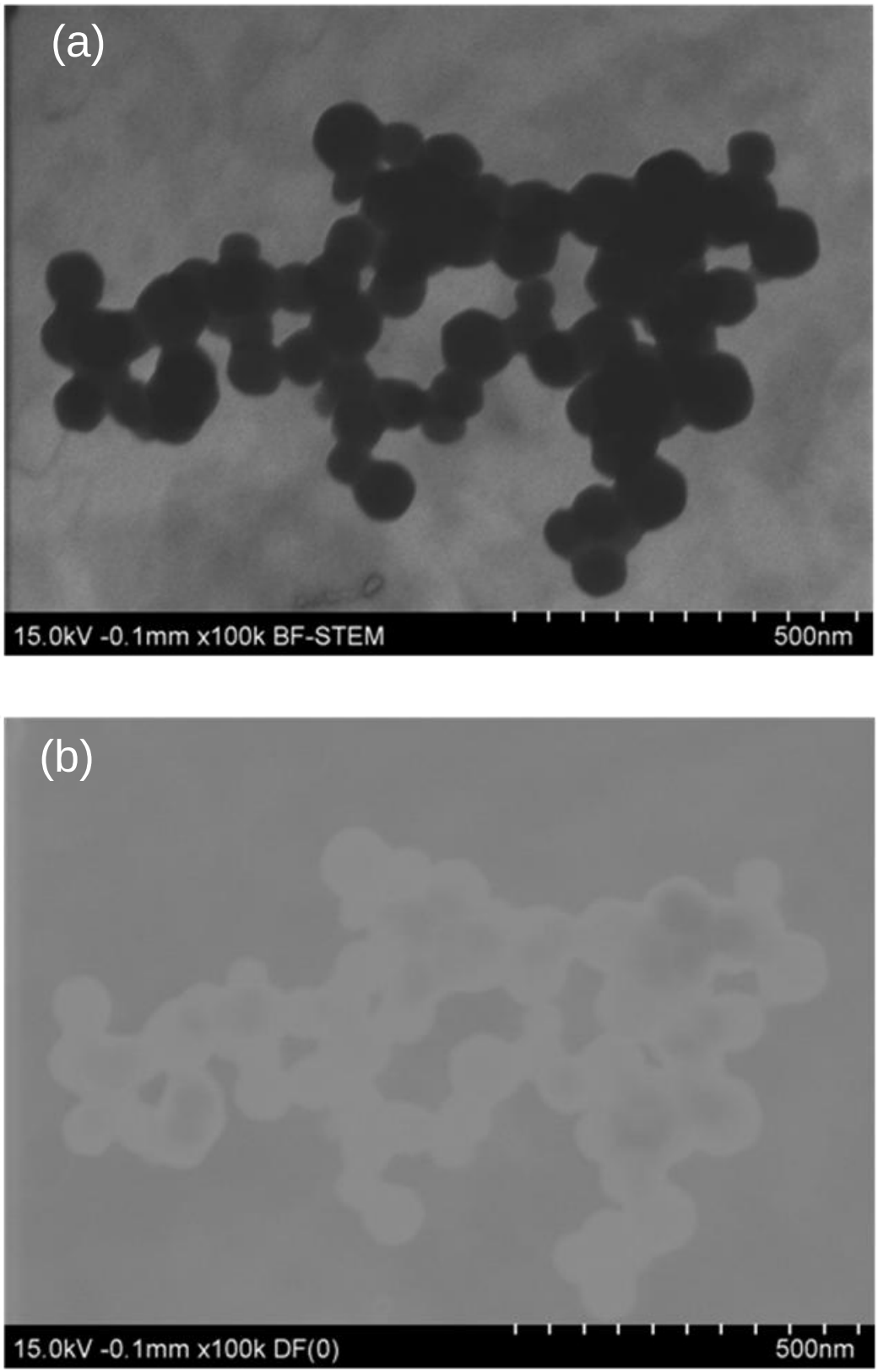

Fig. S5 STEM micrographs of the ZIF-8 nanoparticles.

N_2 adsorption and desorption

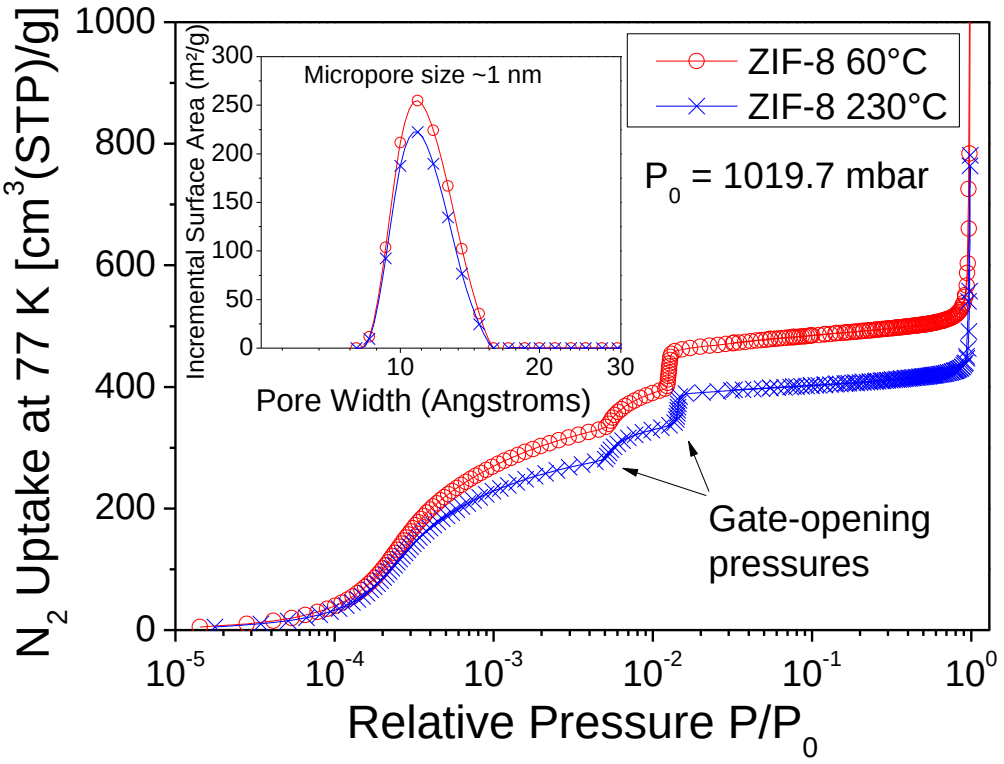

Fig. S6 N_2 adsorption isotherms of the ZIF-8 nanoparticles annealed at 60°C and 230°C for 18h. The inset shows the pore size distribution calculated by non-linear DFT model. Micropores were evacuated at 60°C under high vacuum of 10^{-6} bar for 24 h.

Table S2 Specific surface area and pore volume of ZIF-8 nanoparticles. Samples were annealed at 60°C and 230°C, respectively.

Sample	BET surface area (m^2/g)	Total pore volume (cm^3/g)	Micropore volume (cm^3/g)
ZIF-8, 60°C	1645	0.77	0.70
ZIF-8, 230°C	1358	0.70	0.58

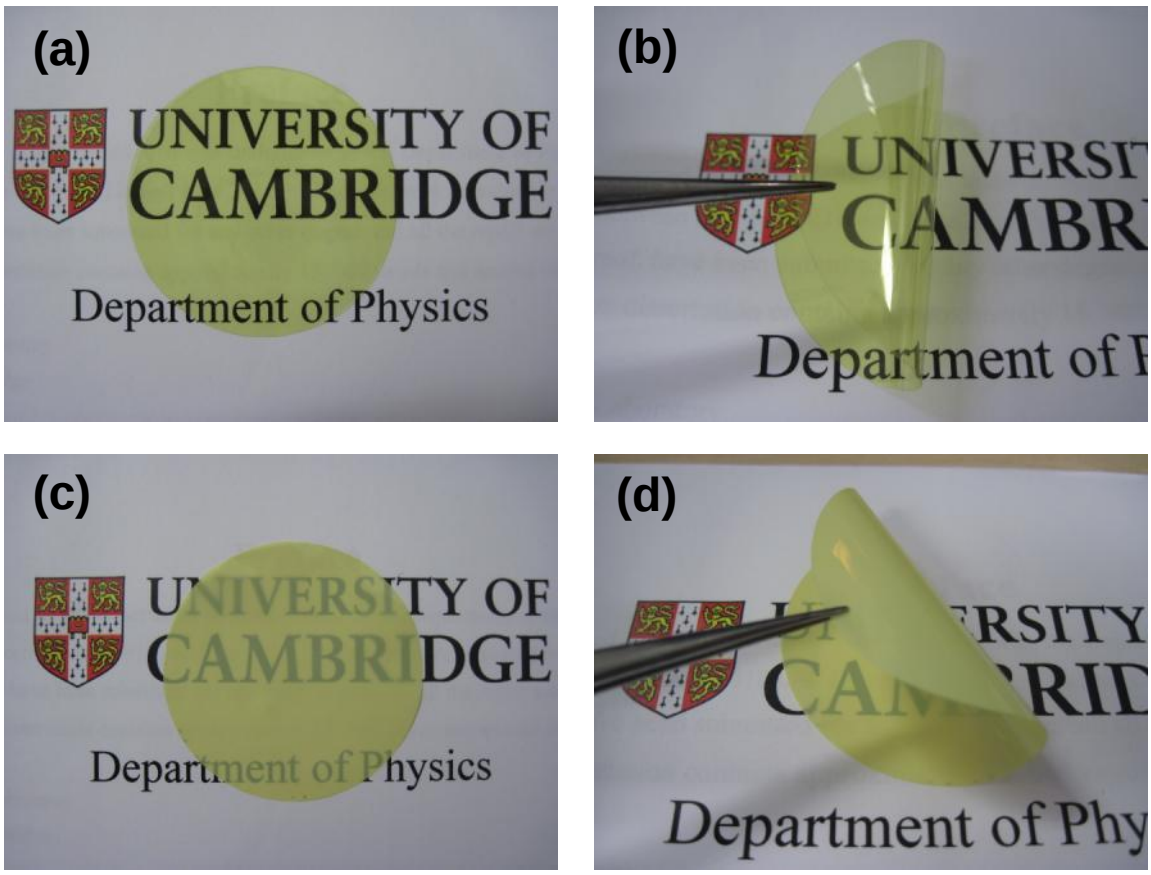

Fig. S7 Photos of (a-b) Matrimid® 5218 polymer membranes and (c-d) Matrimid®/ZIF-8 nanocomposite membrane with 20wt% loading annealed at 150°C. The diameter of membrane is 47 mm.

Cross-section morphology of membrane

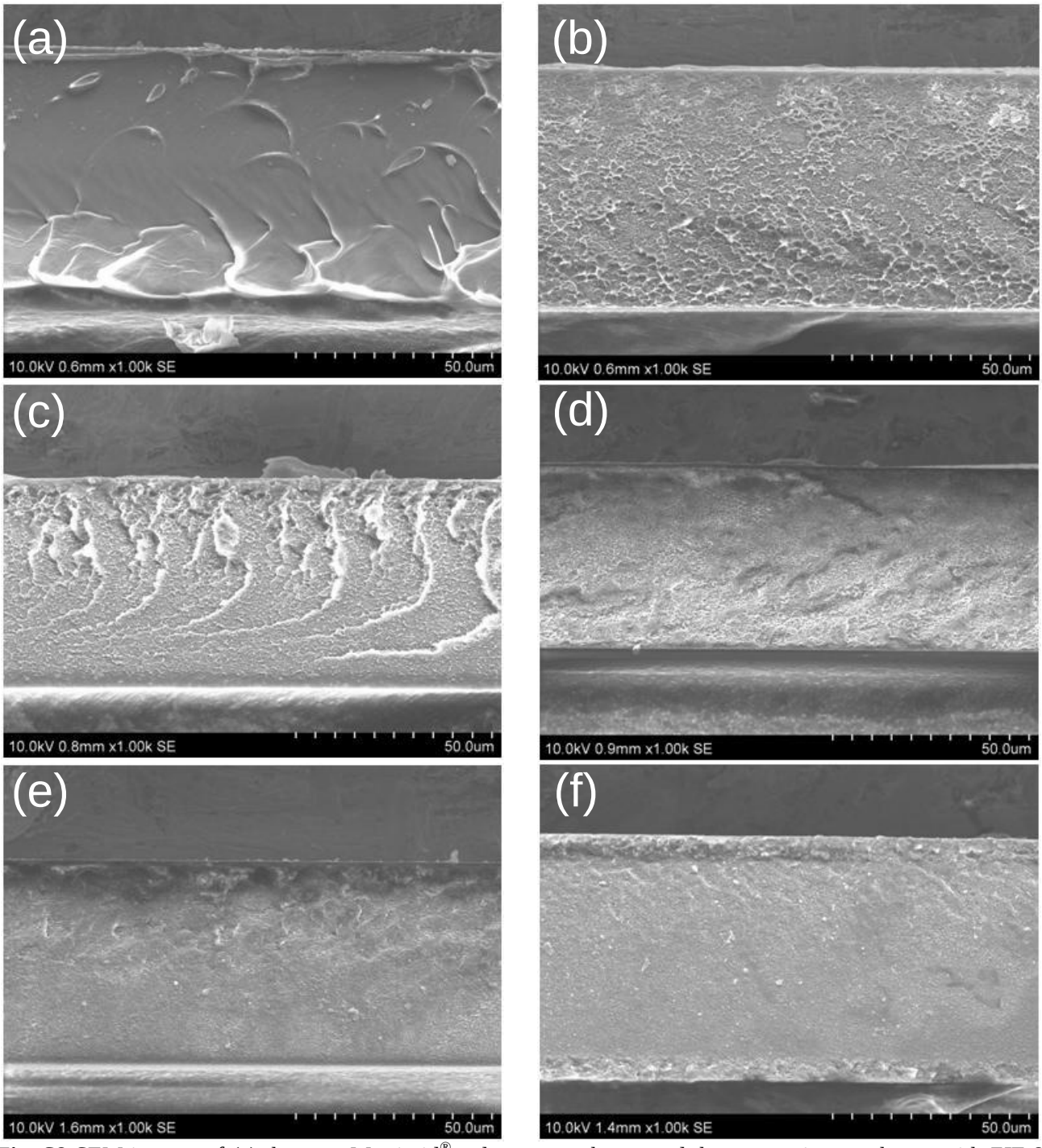

Fig. S8 SEM images of (a) the pure Matrimid® polymer membrane and the composite membrane with ZIF-8 loading of (b) 5wt%, (c) 10wt%, (d) 20wt%, (e) 30wt%, (f) 40wt%. All membranes were annealed at 230°C for 18 h under vacuum. The low magnification SEM micrographs show the morphologies of whole cross-section of the membrane.

XRD patterns

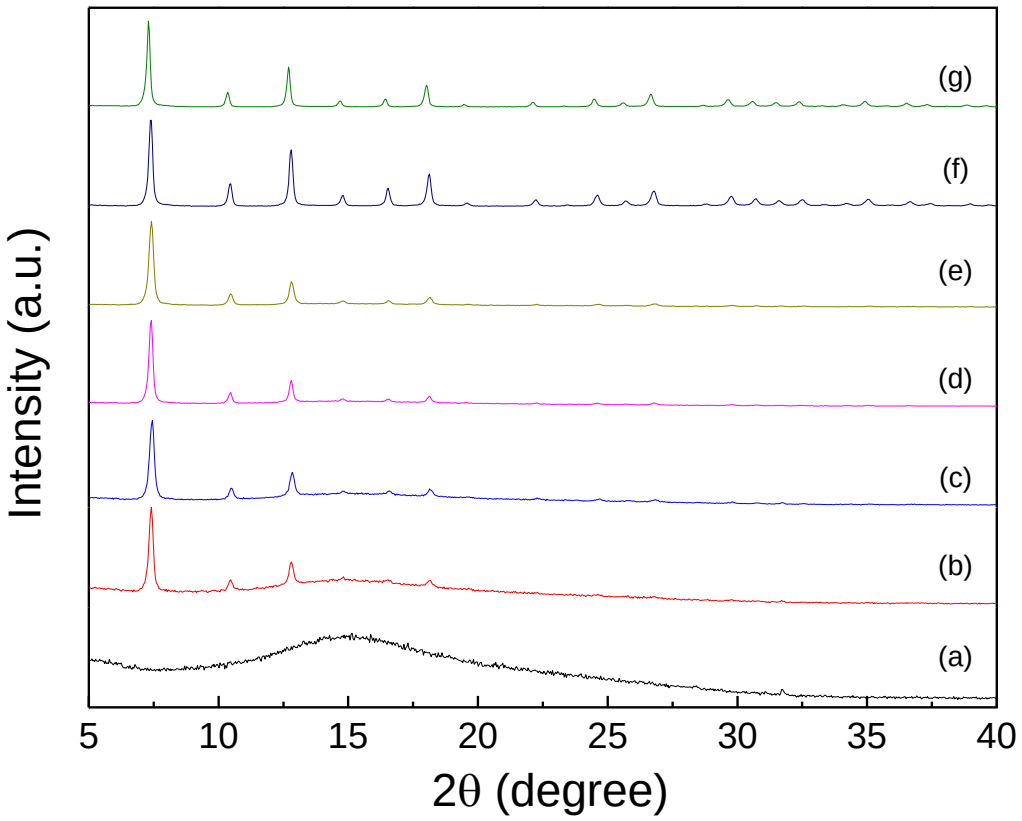

Fig. S9 X-ray diffraction patterns of (a) pure Matrimid® 5218, in contrast to composite membrane containing ZIF-8 nanoparticles with loading of (b) 5 wt%, (c) 10 wt%, (d) 20 wt%, (e) 30 wt%, and (f) ZIF-8 nanocrystals annealed at 230°C under vacuum, and (g) ZIF-8 nanocrystals dried at 60°C under vacuum.

FTIR analyses

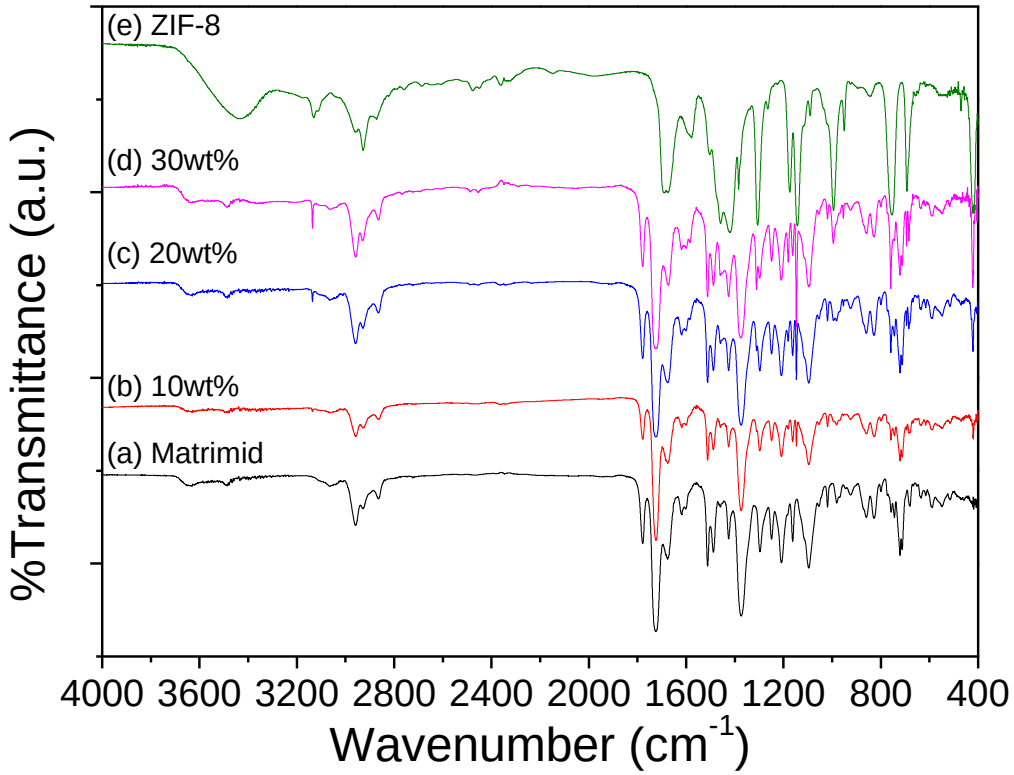

Fig. S10 FTIR analysis of pure Matrimid® and Matrimid®/ZIF-8 mixed matrix membrane with loadings marked above the curves. All samples were annealed at 230°C for 18 h under vacuum.

FTIR analyses of pure ZIF-8, pure polymer, and composite membranes were performed as shown in Fig. 7. The spectrum of pure ZIF-8 matches well the pattern reported in the literature. [11] The absorption bands at 421 cm^{-1} is due to the Zn-N stretching. The peaks found between 900-1400 cm^{-1} are associated with the absorption of C-N bonds. The absorption bands at 2928 cm^{-1} and 3134 cm^{-1} are associated with the aromatic C-H stretching and the aliphatic C-H stretch of the imidazole. The peaks of pure Matrimid® also match the literature well.[12] For the Matrimid/ZIF-8 composite membrane, we do not see fundamental OH stretching vibration (typically a broad peak centred between 3600-3000cm^{-1}). We see this peak in the sample of pure ZIF-8, which could be possibly due to the adsorption of moisture during preparation of the KBr platelet. All the peaks of Matrimid®/ZIF8 composite film could be assigned to ZIF-8 and Matrimid®, respectively, indicating that there were not strong chemical interactions between the ZIF-8 nanoparticles and the polymer.

Glass transition temperature by dynamic mechanical analyses (DMA)

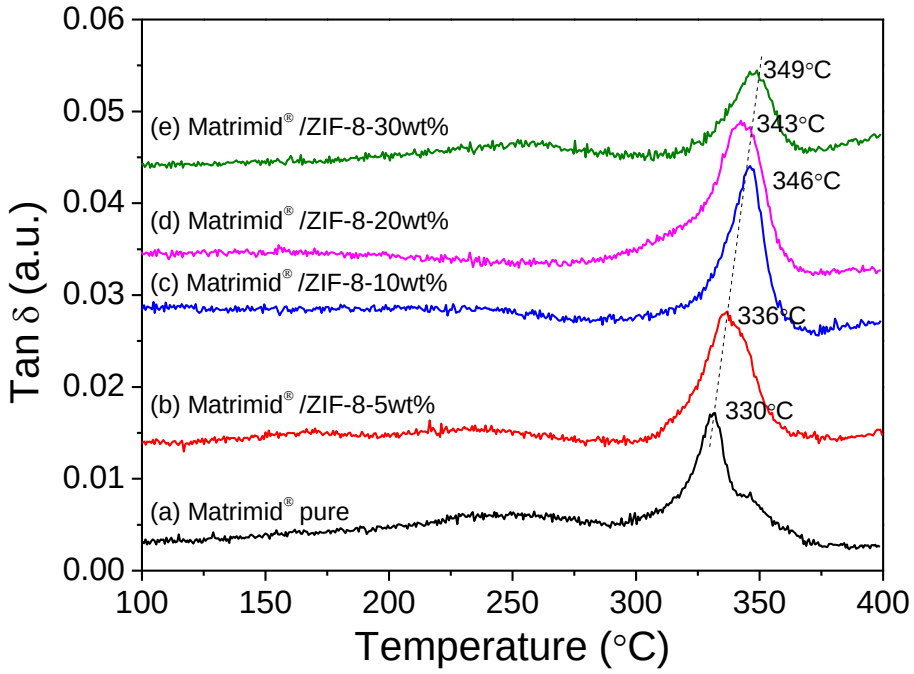

Fig. S11 The ratio of storage modulus to the loss modulus, or tan (δ) as a function of temperature, for pure Matrimid® membrane and Matrimid®/ZIF-8 nanocomposite membrane with loading of 5-30wt% measured by DMA.

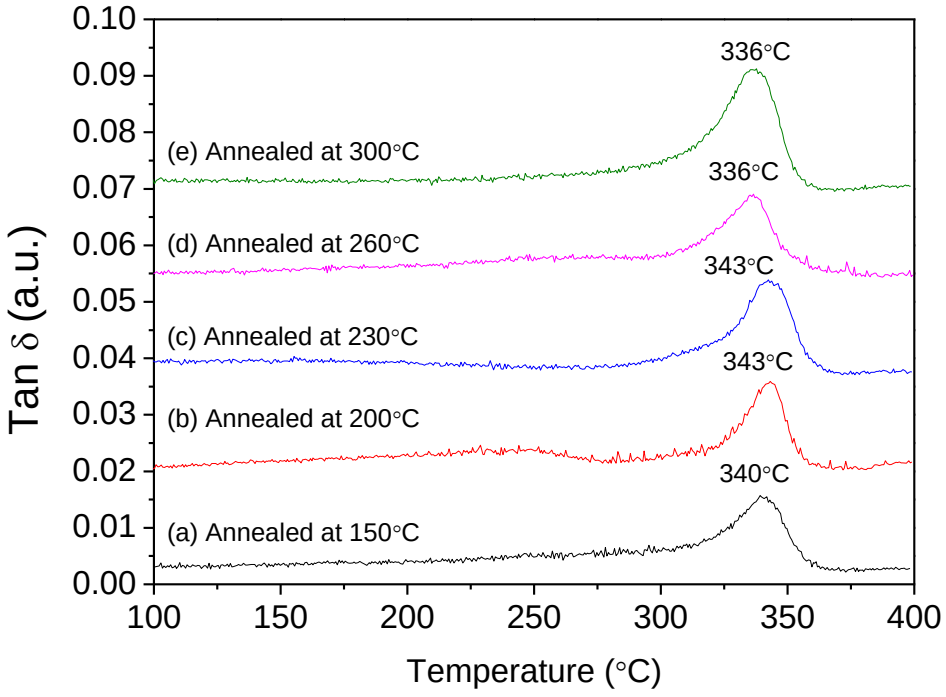

Fig. S12 The ratio of storage modulus to the loss modulus, or tan (δ) as a function of temperature, for Matrimid®/ZIF-8 nanocomposite membrane with ZIF-8 loading of 20 wt% annealed at various temperatures (as marked) measured by DMA.

Table S3 Gas permeation properties of the Matrimid® membrane under varied annealing temperature under vacuum for 18h. Gas permeation test condition: feed pressure of 4 bar at room temperature (22°C). 1 Barrer = 10^{-10} cm^3 (STP) cm/(cm^2 s cmHg).

Sample	Permeability (Barrer)					Selectivity				
	H_2	CO_2	O_2	N_2	CH_4	CO_2/N_2	CO_2/CH_4	O_2/N_2	H_2/N_2	H_2/CH_4
Matrimid®- 60°C	11.81	13.64	4.07	0.82	0.97	16.6	14.1	5.0	14.4	12.2
Matrimid®- 150°C	24.64	6.68	2.14	0.33	0.29	20.1	23.3	6.4	74.0	85.8
Matrimid®- 180°C	28.03	7.43	2.20	0.31	0.24	24.3	31.5	7.2	91.7	118.8
Matrimid®- 200°C	28.48	7.06	2.20	0.31	0.20	22.6	34.6	7.0	91.1	139.6
Matrimid®- 230°C	32.68	8.07	2.62	0.36	0.23	22.4	35.2	7.3	90.9	142.7
Matrimid®- 260°C	27.69	6.29	2.19	0.28	0.19	22.6	33.8	7.9	99.5	148.6
Matrimid®- 300°C	27.78	6.60	2.07	0.29	0.20	22.6	33.8	7.1	94.9	142.3

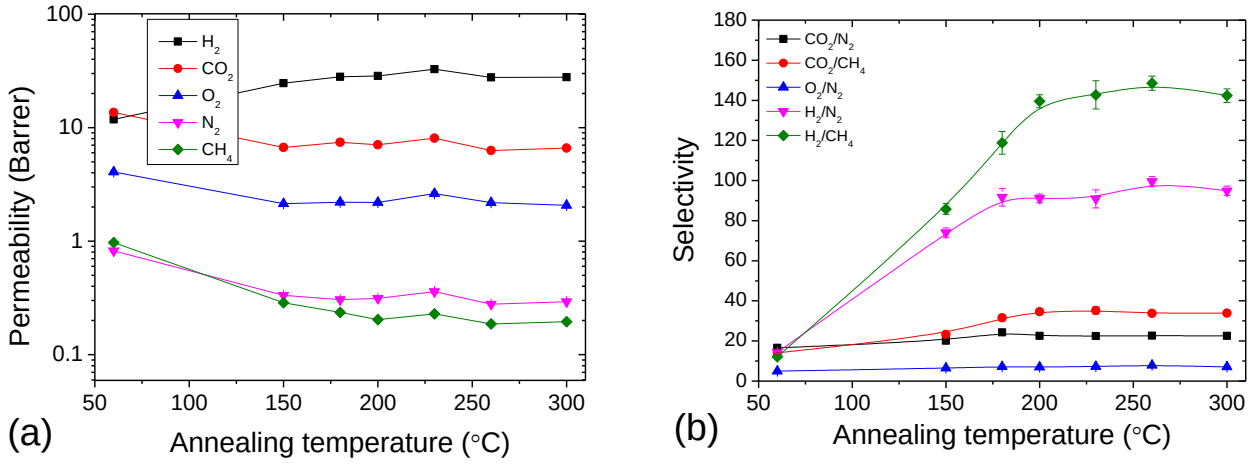

Fig. S13 Effect of annealing temperature on the pure gas permeation properties of pure Matrimid® 5218 membrane. (a) permeability and (b) selectivity of gas pairs.

The effect of annealing temperature on the gas permeation properties of pure Matrimid® membrane was investigated, as shown in Table S3 and Fig.S13, as control for the composite membrane. The residual solvent could has significant effect on the molecular packing and gas permeation properties of the membrane. With the annealing temperature increased to around 200°C, the permeability of H_2 increased to around 30 Barrer, while the permeabilities of CO_2, O_2, N_2 and CH_4 decreased slightly and stabilised when the temperature was above 200°C. Furthermore, the selectivities of corresponding gas pairs increased and stabilised.

Table S4 Gas permeation properties of the Matrimid®/ZIF-8 nanocomposite membrane with 30wt% loading of ZIF-8 nanoparticles annealed at various temperature for 18 h under vacuum. Gas permeation test condition: feed pressure of 4 bar at room temperature (22°C). 1 Barrer = 10^{-10} cm^3 (STP) cm/(cm^2 s cmHg).

Sample	Permeability (Barrer)					Selectivity				
	H_2	CO_2	O_2	N_2	CH_4	CO_2/N_2	CO_2/CH_4	O_2/N_2	H_2/N_2	H_2/CH_4
Matrimid®/ZIF-8-30wt%-150°C	113.31	9.10	13.57	9.21	8.70	1.0	1.0	1.5	12.3	13.0
Matrimid®/ZIF-8-30wt%-180°C	115.83	29.24	11.17	2.00	1.17	14.6	25.1	5.6	58.0	99.3
Matrimid®/ZIF-8-30wt%-200°C	117.33	27.50	10.51	1.54	0.97	17.8	28.3	6.8	76.0	120.7
Matrimid®/ZIF-8-30wt%-230°C	112.06	28.72	10.18	1.68	1.16	17.1	24.9	6.1	66.8	97.0
Matrimid®/ZIF-8-30wt%-260°C	98.92	21.35	7.61	1.08	0.73	19.8	29.3	7.1	91.9	135.5
Matrimid®/ZIF-8-30wt%-300°C	144.51	29.19	10.65	4.43	4.60	6.6	6.3	2.4	32.6	31.4

Diffusion coefficient and solubility of gas molecules in polymer and composite membranes

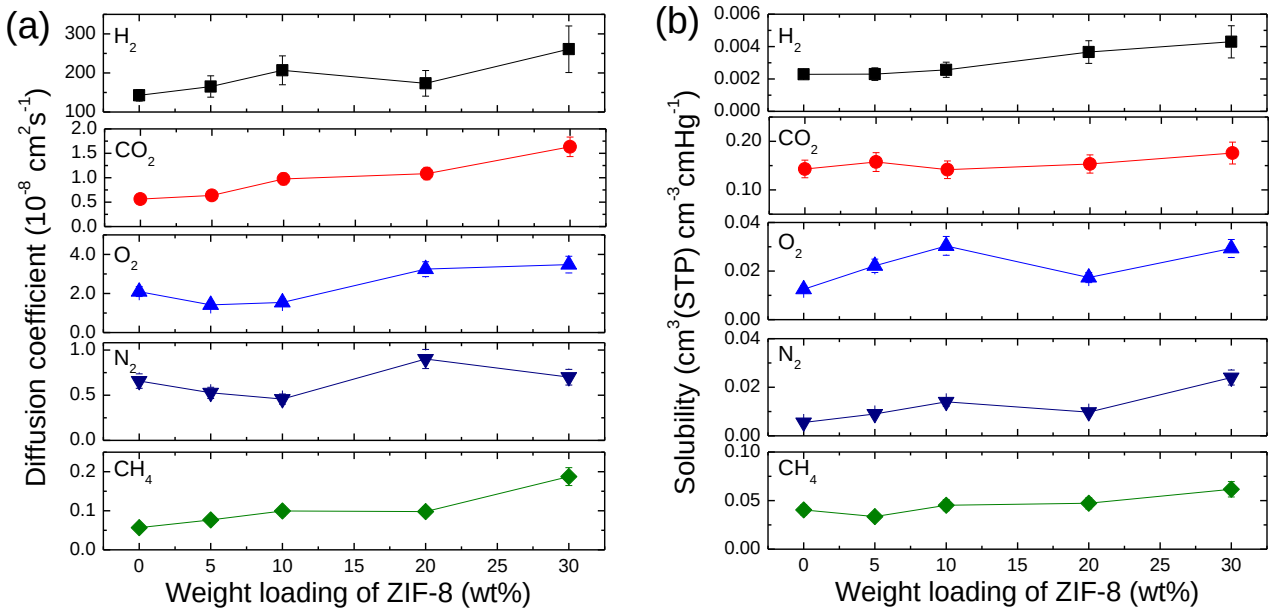

Fig. S14 Apparent (a) diffusion coefficients and (b) solubility of gases in Matrimid®/ZIF-8 mixed matrix membrane with various loadings of ZIF-8. Membranes were annealed at 230°C for 18h under vacuum.

Further information on Positron Annihilation Lifetime Spectroscopy (PALS)

In PALS experiments, a positron is injected into the material being tested and the length of time until that positron annihilates with one of the material's electrons is measured. When a positron enters a molecular material, it thermalises within a few picoseconds, after which, it may diffuse through the material over a mean free path of a few nm, either as a free particle and self annihilate directly, or capture an electron to form a positronium-atom.[13-14] Positronium (Ps) is an electron-positron bound state with two spin states: *para*-positronium (*p*-Ps), a singlet state with zero spin angular momentum (the electron and positron have anti-parallel spins); and *ortho*-positronium (*o*-Ps), a triplet state of unit spin angular momentum (the electron and positron have parallel spins). In vacuum, due to the relative number of states available, the population of the two Ps spin states is *o*-Ps: *p*-Ps = 3:1 and *p*-Ps and *o*-Ps annihilate intrinsically with mean lifetimes of 0.125 ns and 142 ns, respectively.[13-14] In molecular materials, Ps localises in the free volume holes between the molecules, where it remains throughout its lifetime. When confined in a local free volume hole, *o*-Ps undergoes numerous collisions with the molecules of the medium, therefore, there is a finite probability that the positron of the *o*-Ps bound state may annihilate with a molecular electron with an opposite spin. This process is known as "pick-off annihilation" and it results in a reduction of the *o*-Ps lifetime with hole size, from 142 ns in an infinitely sized hole (*o*-Ps self-annihilation in vacuum) to 1 - 4 ns for sub-nanometer sized holes.[13-14] The lifetime of *o*-Ps is, therefore, environment dependent and it delivers information pertaining to the size of the local free volume hole in which it resides.

Four discrete lifetimes were resolved in the PALS spectra measured for all Matrimid® based membranes at 25 ºC but in the main text we only discuss the two longer components attributed to *o*-Ps annihilation. It is worth mentioning that the two shorter lifetimes, $\tau_{p\text{-}Ps}$ ~ 0.20 ns and τ_{e+} ~ 0.40 ns, attributed to annihilation from *p*-Ps and free positron states, respectively (lifetimes are in agreement with the values reported for common polymers[13-14]) were found to be independent of the ZIF-8 loading level.

In Table 1 we also present the *o*-Ps intensities measured for the Matrimid® based membranes, which represent the relative number of positrons annihilating from each of the two *o*-Ps states. These parameters reflect the probability of *o*-Ps formation, which in molecular materials is related to the number of sites (free volume elements) available for Ps formation, as well as the chemical parameters governing the mechanism of Ps formation. The individual *o*-Ps intensities (as well as their sum which reflects the total relative number of

positrons annihilating from an *o*-Ps state) measured for the Matrimid® based membranes are significantly lower than the *o*-Ps intensities measured for common polymers. Similar observations have been previously reported for a number of polyimide based materials, for which *o*-Ps intensities in the range of 0.5 -17 % have been measured and in some cases the long-lived *o*-Ps component was absent all together.[15-17] In general, polyimides are known to strongly suppress (inhibit) the formation of Ps and the inhibition effect is principally governed by the chemistry of the di-anhydride. Taking this into consideration, it must be noted that the *o*-Ps intensities measured do not directly correspond to the concentration of free volume elements in the Matrimid® based membranes.

References

1. R. W. Baker, *Membrane Technology and Applications*, John Wiley & Sons, Ltd, 2004.
2. Y. S. Li, F. Y. Liang, H. Bux, A. Feldhoff, W. S. Yang and J. Caro, *Angew. Chem., Int. Ed.*, 2010, **49**, 548-551.
3. Y. Li, F. Liang, H. Bux, W. Yang and J. Caro, *J. Membr. Sci.*, 2010, **354**, 48-54.
4. H. Bux, F. Liang, Y. Li, J. Cravillon, M. Wiebcke and J. Caro, *J. Am. Chem. Soc.*, 2009, **131**, 16000-16001.
5. M. C. McCarthy, V. Varela-Guerrero, G. V. Barnett and H. K. Jeong, *Langmuir*, 2010, **26**, 14636-14641.
6. H. Bux, A. Feldhoff, J. Cravillon, M. Wiebcke, Y. S. Li and J. Caro, *Chem. Mater.*, 2011, **23**, 2262-2269.
7. A. Huang, H. Bux, F. Steinbach and J. Caro, *Angew. Chem., Int. Ed.*, 2010, **49**, 4958-4961.
8. A. Huang, W. Dou and J. Caro, *J. Am. Chem. Soc.*, 2010, **132**, 15562-15564.
9. A. Huang and J. Caro, *Angew. Chem., Int. Ed.*, 2011, **50**, 4979-4982.
10. K. S. Park, Z. Ni, A. P. Côté, J. Y. Choi, R. Huang, F. J. Uribe-Romo, H. K. Chae, M. O'Keeffe and O. M. Yaghi, *Proc. Natl. Acad. Sci. U. S. A.*, 2006, **103**, 10186-10191.
11. J. Cravillon, S. Münzer, S. J. Lohmeier, A. Feldhoff, K. Huber and M. Wiebcke, *Chem. Mater.*, 2009, **21**, 1410-1412.
12. M. J. C. Ordoñez, K. J. Balkus, J. P. Ferraris and I. H. Musselman, *J. Membr. Sci.*, 2010, **361**, 28-37.
13. Y. C. Jean, P. E. Mallon and D. M. Schrader, *Positron and positronium chemistry*, World Scientific: River Edge, NJ, 2003.
14. D. M.Schrader and Y. C. Yean, *Positron and positronium chemistry*, Elsevier, Amsterdam, 1988.
15. K.-i. Okamoto, K. Tanaka, M. Katsube, O. Sueoka and Y. Ito, *Radiat. Phys. Chem.*, 1993, **41**, 497-502.
16. V. P. Shantarovich, T. Suzuki, C. He, Y. Ito, Y. P. Yampolskii and A. Y. Alentiev, *Radiat. Phys. Chem.*, 2005, **73**, 45-53.
17. J. Kruse, J. Kanzow, K. Rätzke, F. Faupel, M. Heuchel, J. Frahn and D. Hofmann, *Macromolecules*, 2005, **38**, 9638-9643.